CO2, CH4 and CO Emission Sources and Their Characteristics in the Lamto Ecological Reserve (Côte d'Ivoire)

Toure Dro Tiemoko *, Fidele Yoroba, Komenan Benjamin Kouassi, Adama Diawara, Kouakou Kouadio, Francois-Xavier Djezia Bella Bouo, Assi Louis Martial Yapo, Abraham Kouman, Michel Ramonet

Posted Date: 5 September 2023

doi: 10.20944/preprints202309.0082.v1

Keywords: CO2; CH4; CO; Bivariate polar diagram; weather conditions; Lamto; Côte d'Ivoire

Article

CO_2, CH_4 and CO emission sources and their characteristics in the Lamto ecological reserve (Côte d'Ivoire)

Dro Touré Tiemoko [1,2,*], Fidèle Yoroba [2,3], Komenan Benjamin Kouassi [2,3], Adama Diawara [2,3], Kouakou Kouadio [2,3], Francois-Xavier Djezia Bella Bouo [1], Assi Louis Martial Yapo [4], Abraham Kouman [3] and Michel Ramonet [5]

[1] Equipe de la Physique pour l'Environnement, Laboratoire de Physique Fondamentale et Appliquée, Université NANGUI ABROGOUA, Abidjan, Côte d'Ivoire ; ttouredro017@gmail.com (D.T.T.); djezia2001@yahoo.fr (F.D.B.B).
[2] Geophysical Station of Lamto (GSL), N'Douci BP 31, Côte d'Ivoire; yorofidele@gmail.com (F.Y); benjamin.kouassi@gmail.com (K.K.B); diawara_adama@yahoo.fr (A.D); kk.kouadio@yahoo.fr (K.K)
[3] Laboratoire des Structures de la Matière, de l'Environnement et de l'énergie Solaire (LASMES), University Felix Houphouet-Boigny, UFR SSMT, Abidjan 22 BP 582, Côte d'Ivoire; bokouman@gmail.com (A.K)
[4] Université Alassane Ouattara, Bouaké, Côte d'Ivoire ; louismartialyapo@gmail.com (A.L.M.Y)
[5] Laboratoire des Sciences du Climat et de l'Environnement (LSCE), IPSL, CEA-CNRS UVSQ, Université Paris-Saclay, Orme des Merisiers, 91191 Gif-sur-Yvette, France ; michel.ramonet@lsce.ipsl.fr (M.R.)
* Correspondence: ttouredro017@gmail.com

Abstract: CO_2, CH_4 and CO are the most critical atmospheric gases in terms of their impact on the radiative system, air quality and health. This work provides information on the direction of source areas and potential sources of emissions and shows many aspects of these gases by a statistical analysis using bivariate polar diagrams and local weather conditions (e.g., temperature, wind speed and wind direction) recorded at the Lamto station (LTO, 6°31N and 5°02W) in Côte d'Ivoire over the 2014-2018 period. The results show that the main regions contributing to the high concentrations of CH_4 (> 1925 ppb) and CO_2 (> 420 ppm) in the GSS, GSP, PSS and PSP seasons are the North and Northwest sectors of Lamto. In these directions, CH_4 and CO_2 concentrations are associated with wind speeds less than 6 $m.s^{-1}$, due to the influences of local sources as emissions resulting from the degradation of organic matter submerged during the impoundment of the Taabo dam, and/nor human activities linked to the practice of intensive agriculture. In addition, the high concentrations of CO (> 350 ppb) are observed in GSS in the North, North-West, North-East and East sectors for wind speeds less than or equal to 9 $m.s^{-1}$, due to the influences of both local and distant sources. The correlation coefficients between CH_4 and CO, and between CH_4 and CO_2 are positive and significant in all sectors. However, those calculated between CO_2 and CO have showed both low and high values in all seasons.

Keywords: CO_2; CH_4; CO; bivariate polar diagram; weather conditions; Lamto; Côte d'Ivoire

1. Introduction

In atmospheric science, the study of the relationships between CO_2, CH_4 and CO, and meteorological parameters on the one hand, correlation and comparison techniques on the other hand are very useful. These techniques allow identifying and characterizing the various sources of these gases [1] and controlling trends through their emission. Moreover, to better distinguish these sources of emission, it is necessary to characterize their spatial and temporal distributions. For this purpose, analysing the wind speed and direction at small and large scales, turbulence and atmospheric stability responsible for the dispersion of the gaseous compounds are important. Emissions processes for these gases are also dependent on ambient (or local) weather conditions because they are influenced by short-wave radiation, temperature, and humidity, etc [2–4].

The correlation between pairs of gases also leads to characterizing sources of emission rather than to studying slopes from regression diagrams [5]. Indeed, Manoli et al. [6] underlined that

analyzes derived from the use of simple and static slopes could be unsuitable in many situations. In addition, some simple techniques analysis (e.g., boosted regression trees, concentration weighted trajectory (CWT), etc.) and of identifications (e.g., non-parametric wind regression (NWR), potential source contribution function (PSCF)) is used and provide important information on sources that are difficult to characterize. The modeling of the receivers is also very used frequently, because it takes into account several aspects for example: the radiative and boundary layer processes, etc ...

This modeling technique has the advantage of identifying and characterizing the sources of emission CO_2, CH_4 and CO. However, given the complexity of some boundary layer processes such as convection and/or turbulence, the air quality models have sometimes difficulty to provide information that allows to better identify and characterize the sources of emission. As a result, in-situ data analysis remains one of the most adequately approaches. Many studies [7–9] have shown that through of innovative technique's application on in-situ data this approach allows much collecting more information. One of these techniques is to statistically analyse the atmospheric concentration levels of species by clustering footprints calculated with the FLEXPART model [10–12]. This technique allows on the one hand to characterise the role of long-range atmospheric transport of air masses and to quantify its impact on the variability of synoptic, seasonal and interannual signals of atmospheric species. On the other hand, to establish source-receptor relationships. Applying this approach on CO_2, CH_4 and CO concentration measured at Lamto over the 2014-2018 period, Tiemoko et al. [12] have shown that high concentrations of these species were observed when the air masses coming exclusively from North-East and North Africa transited through some West African countries (Ghana, Togo, Benin, Nigeria, Niger, Burkina-Faso). These authors have shown that these continental emissions explain ~40%, ~74% and ~66% of the variances of CO_2, CH_4 and CO, respectively. The results of this study have led to specific conclusions and highlighted the impacts of distant emission sources. However, in order to explain the totality of the CO_2, CH_4, and CO variances on the site, it is necessary to also take into account the local impacts. as those resulting to the presence of the Taabo dam near the Lamto station. Indeed, Rosa and Schaeffer. [13], Galy-Lacaux et al. [14,15] and Delmas et al. [16] point out that these emissions have proven to be significant in a tropical environment.

These facts show here the necessity of using another innovative technique which is the bivariate polar diagram [17,18] through the package Openair [19] for the R programming environment. This bivariate method, which takes into account the local meteorological conditions, in particular wind speed and direction, is effective to determine potential emission directions of the gases and to determine correlations between the gases for each wind sector. It is now widely used by a large part of the scientific community for the air quality and climate change studies [20]. These applications have shown good results in the determination study of the potential source of emission of gases [21,22] and also atmospheric pollutants [23,24].

This study aims to analyze the temporal relationships existing between local meteorological parameters and CO_2, CH_4 and CO, known for their significant contributions to radiative forcing [25]. We will therefore identify the trends of their variations as well as the probable causes of the high concentrations measured sometimes at the LTO station over the 2014-2018 period, using the Openair package functions in the R environment.

This work is structured as follows; Section 2 describes the study area, data and methods used. Section 3 presents the results and discussions. Finally, we conclude and give some perspectives to the future improvement of the work.

2. Material Data and Method

2.1. Study area

The region of Lamto (5°02W and 6°13N) is in an equatorial transition climate [26]. Indeed, to simplify, Devineau. (1975) underlines that the rainfall regime at Lamto is governed by a struggle influence between the monsoon in the south and harmattan in the north. In the confluence area, the moist air (i.e., monsoon) is more or less depressed under the hot and dry air mass (i.e., harmattan). The delimitation zone at the ground between these two air masses is the Intertropical Front (F.I.T)

 doi:10.20944/preprints202309.0082.v1

and it is inclined from south to north. This front moves from south to north and from north to south during the year in relation with the thermal equator [28] and it provides at Lamto a rainfall regime of four-seasons (i.e., two rainy seasons and two dry seasons).

The main rainy season is from March to July (GSP) while the short rainy season is from September to November (PSP). Then main dry season appears from December to February (GSS) while the short dry season (PSS) is confined in PSS. The mean annual rainfall amount and temperature are 1200 mm and 27°C respectively. The vegetation is mainly wet savannah (80% of the area) and forest (20% of the area). Anthropogenic activities are those related to agriculture, fishing and livestock farming. The Lamto region is influenced by annual passes of bush fires destroying about 80% of the aboveground biomass [29].

2.2. Data

The database used in this work is a homogeneous temporal serie of meteorological parameters (ground-base) as temperature and wind speed and direction, and CO_2, CH_4 and CO concentrations recorded simultaneously over the 2014-2018 period at Lamto. CO_2, CH_4 and CO concentrations were measured using the CRDS_Picarro_G2401 instrument. This instrument model, based on hollow ring spectroscopy, has linear and stable responses, and it is recognized for its high accuracy in measuring the molar fractions of CO_2 (ppm), CH_4 (ppb) and CO (ppb). Continuous measurements are calibrated to the international reference scale of the World Meteorological Organization (WMO) using six calibration tanks from the Laboratory of Climate and Environmental Sciences (LSCE). The air analyzed is taken continuously at the top of a 50 m tower. The measuring system, data processing, and calibration strategy are explained by Tiemoko et al. [4,12].

2.3. Methods

2.3.1. Bivariate polar plots

Bivariate polar diagrams show how a concentration of a gas varies with both wind speed and direction in polar coordinates [18]. These diagrams have shown their performance in a variety of situations, such as characterization of airport sources and characteristics of dispersion in "canyon" streets (i.e., streets subject to atmospheric releases from traffic) (Carslaw and Ropkins, 2012). Wind direction and speed can be very important in discriminating various sources of emission (Carslaw and Beevers, 2013). The diagrams use a useful graphical technique that can provide directional information on sources as well as concentration dependence on wind speed or temperature from polar coordinates [20].

To simplify, the bivariate polar diagrams are constructed in the following way: first, the wind speed and direction, and concentrations data are divided into classes of wind speed and direction, and mean concentrations calculated for each class. The wind components are explained by equation 1:

$$u = \bar{u}\sin(\frac{2\pi}{\theta});\ v = \bar{u}\cos(\frac{2\pi}{\theta}) \qquad (1)$$

where $\bar{u}$ is the mean hourly wind speed, θ is the mean wind direction in degrees with origin 90°E and C the provided concentration at the surface. The above relations provide the surface data u, v and the concentration (C).

2.3.2. Bivariate CPF methodology

The Conditional Probability Function (CPF) [32] analyzes the impacts of point sources from different directions and wind speeds. It estimates the probability so that the measured concentration exceeds a fixed threshold for a given wind sector [32–34] while determining the direction of the source zones that significantly affect the receptor site [35]. In this study, 4 wind sectors (i = 90 degrees) were chosen and the threshold values were fixed at the 85th percentile over the entire study period in the

 doi:10.20944/preprints202309.0082.v1

4 seasons of the Lamto rainfall regime. The threshold percentile choice here takes into account the distribution of concentrations as a function of wind speed and direction, and also the trend of CO_2, CH_4 and CO species obtained at Lamto area by Tiemoko et al. [12] over the 2014-2018 period. The CPF function is defined by:

$$CPF_{\Delta\theta} = \frac{m_{\Delta\theta/C\geq X}}{n_{\Delta\theta}} \quad (2)$$

where $m_{\Delta\theta}$ is the number of samples or the number of exceeded pollution threshold in the wind sector $\Delta\theta$, the concentration C is greater than or equal to a threshold value X, and $n_{\Delta\theta}$ is the total number of samples or the total number of hourly data from the same wind sector $\Delta\theta$.

3. Results et Discussion

3.1. Local Meteorology

The wind regime (Figure 1) shows a predominance of the south and southwest winds sectors during the GSP, PSS and PSP seasons of the rainfall regime over the 2014-2018 period. The presence of these winds from the south and southwest sectors shows the significant influence of the monsoon flow in the region. However, in GSS season, the predominant winds are observed in three different sectors (i.e., south, southwest and northwest). In contrast, Lamto does not show predominant winds in the northeastern sector, where there are highest wind speed values. Northeast winds are characteristic of the harmattan flow in the GSS season [36,37]. Winds from the southwestern sector are majority and their frequency of occurrence is about 27%.

To compare quantitatively the variation in wind speed over the 4 seasons, statistics including the hourly average, minimum and maximum values of wind speed are presented in Table 1. Average hourly small-scale wind speeds observed are 2.48, 2.49, 2.55 and 2.21 m. s^{-1} in GSS, GSP, PSS and PSP respectively, indicating the existence of relatively weak advection conditions affecting Lamto area. Indeed, Adler et al. [38] during the DACCIWA (West Africa) ground-based field campaign emphasize that advection conditions are considered weak when average wind speed is inferior to 3 m. s^{-1}. The maximum wind speed was 11.15 m. s^{-1} in GSP, which was 4%, 15% and 20% higher than in GSS, PSS and PSP respectively. Minimum wind speed was quite similar for all four seasons.

Figure 2 shows average diurnal cycle of temperature (a), wind speed (b), and wind direction (c) during the 4 seasons of rain regime (GSS, GSP, PSS, and PSP) over the 2014-2018 period at Lamto. Temperature shows pronounced seasonal diurnal cycles with average amplitudes of ~9.3°C; 6.63°C; 5.09°C and 6.55°C in GSS, GSP, PSS and PSP respectively (see Table 2). These amplitude values indicate that during GSS, the temperature variations are significantly larger than the other 3 seasons, which show almost similar diurnal variations. Thus, high magnitude value observed during the GSS could be due to the fact that this season is subject to favorable conditions for the rapid increase (fires) and decrease (Harmattan) in temperature on a diurnal scale. During all the seasons, average hourly minimum temperature was observed in early morning (05:00 to 06:00 local time), while the maximum value in the early afternoon (14:00 to 16:00 local time). Moreover, diurnal cycles of wind speed (Figure 2b) show two significant peaks at around 9:00 am and 7:00 pm and minimums in the early morning (6:00 am to 8:00 am local time) and in the afternoon (1:00 pm to 3:00 pm local time) during the different seasons. The wind speed minimum is in phase with the temperature minimum, while the wind speed maximum occurs about three hours after the afternoon temperature maximum. As for the amplitude values (Table 2), we observe low and quasi-similar average values, indicating a less significant change from one season to another in wind speed on a diurnal scale. Since the diurnal cycles of wind speed and temperature are quite pronounced during the different seasons, it was evident that the trend of day and night data of CO_2 and CH_4 highly dependent on these environmental parameters at an hourly scale would be significantly different. On Figure 2c, it clearly appears that the diurnal cycle of wind direction in GSS is well pronounced (Table 2) as for temperature (Figure 2a). During this season, the minimum value of wind direction is reached between 00:00 and 02:00 local time, associated with an average direction between 150 and 162° (south-east), while the maximum observed between 15:00 and 17:00 local time is associated with an average direction between 250° and 260° (south-west).

Preprints (www.preprints.org) | NOT PEER-REVIEWED | Posted: 5 September 2023 doi:10.20944/preprints202309.0082.v1

However, GSP, PSS, and PSP show diurnal cycles of wind direction that vary very little from one time of day to another and also from one season to another.

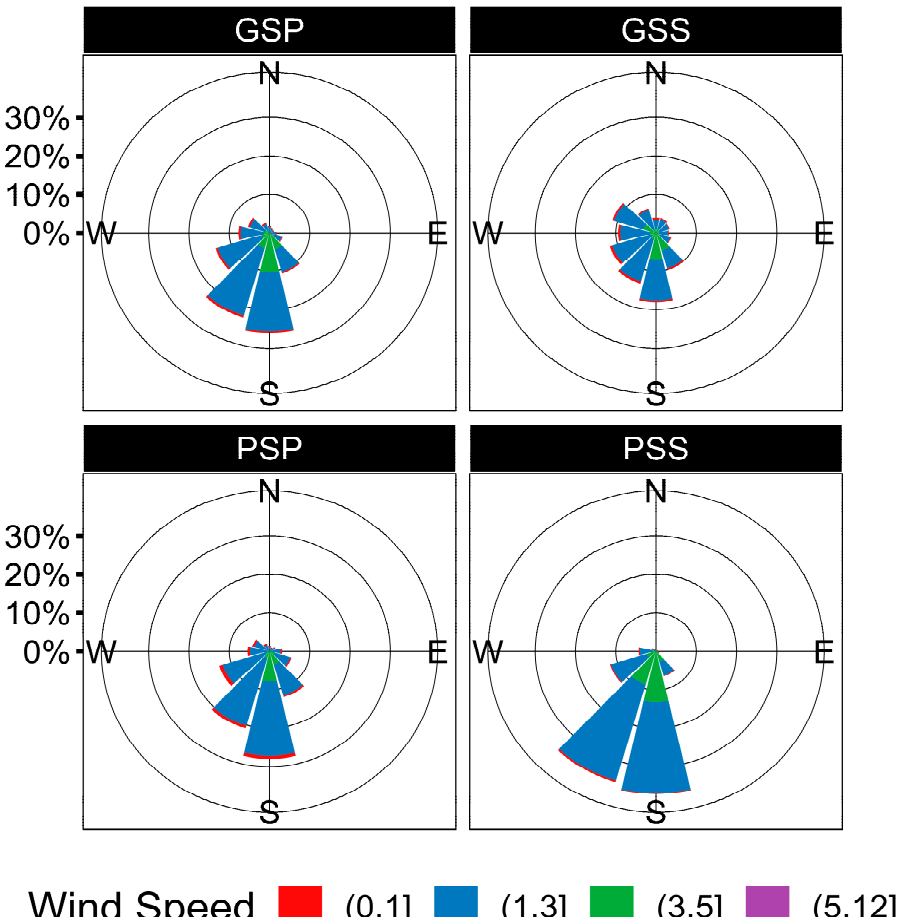

Figure 1. Seasonal wind roses over the 2014-2018 period at Lamto. GSP, GSS, PSP and PSS are the great wet, the great dry, the short-wet and the short dry seasons, respectively. Colors indicate the wind speed scale (in ms^{-1}).

Table 1. Wind data statistics for the four seasons GSS, GSP, PSS and PSP.

	Wind Speed ($m.s^{-1}$)		
Seasons	**Average**	**Minimum**	**Maximum**
GSS	2.48	0.21	10.84
GSP	2.49	0.15	11.15
PSS	2.55	0.26	9.36
PSP	2.21	0.23	8.35

Table 2. Diurnal seasonal amplitudes of temperature and wind speed during the 4 seasons (GSS, GSP, PSS, and PSP) of the rainfall regime in Lamto over the 2014-2018 period.

	Diurnal amplitude	
Seasons	**Temperature (°C)**	**Wind Speed ($m.s^{-1}$)**
GSS	9.30	1.26
GSP	6.63	1.52
PSS	5.09	1.65
PSP	6.55	1.34

Preprints (www.preprints.org) | NOT PEER-REVIEWED | Posted: 5 September 2023 doi:10.20944/preprints202309.0082.v1

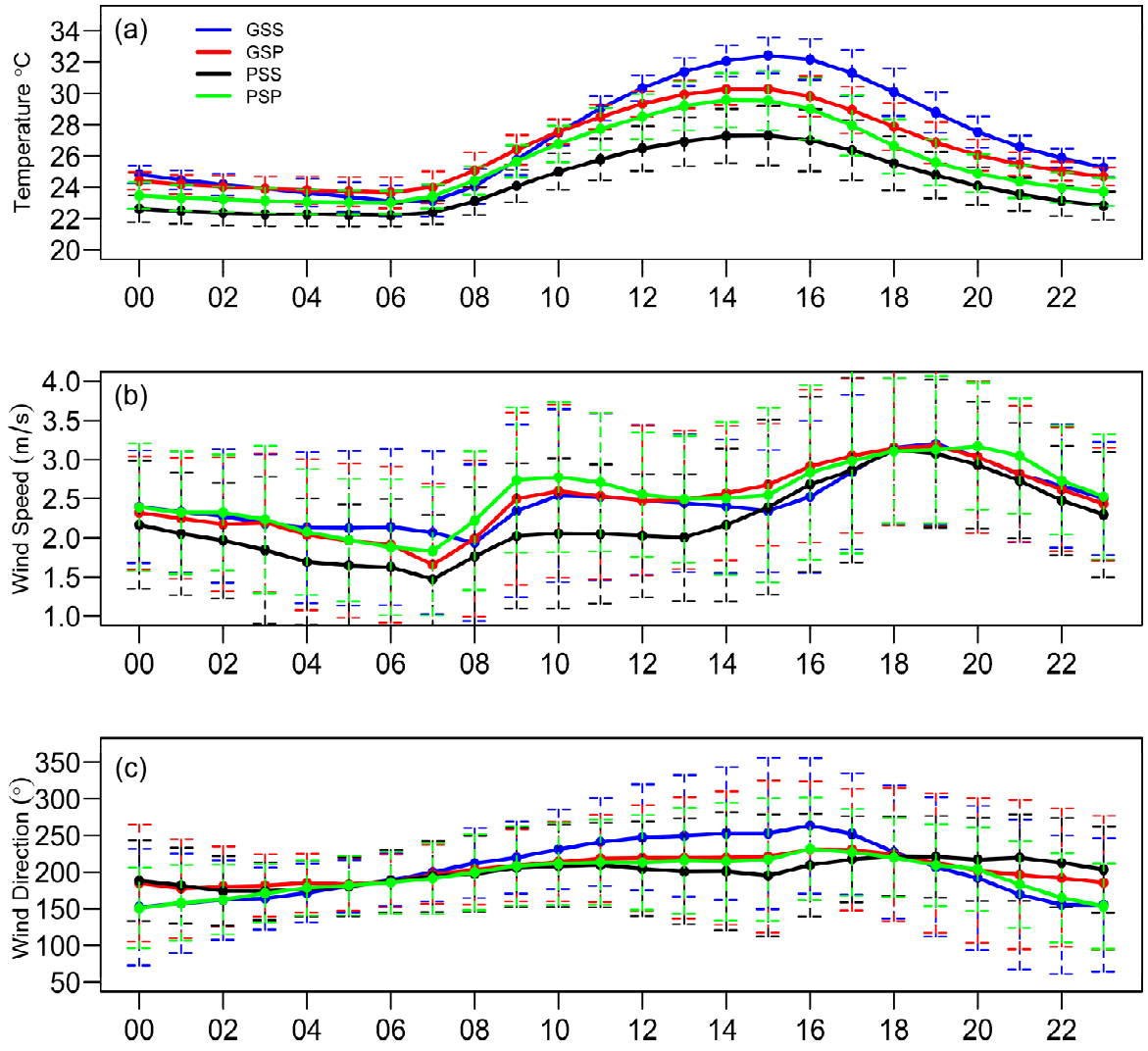

Figure 2. Seasonal diurnal cycles of (a) Temperature, (b) Wind speed and (c) Wind direction measured at Lamto (GMT) over the 2014-2018 period. Vertical bars represent standard deviation.

3.2. CPF and bivariate polar plots

3.2.1. CH_4

Figure 3 shows polar diagrams with two variables (i.e., temperature and wind direction, wind speed and wind direction) and the CPF of CH_4 during the 4 seasons of the rainfall regime (i.e., GSS, GSP, PSS and PSP) at Lamto. Figure 3a show that high values of concentrations of CH_4 (> 1850 ppb) come from the northwestern and northeastern sectors where there are agricultural areas and the Taabo hydroelectric dam except for the PSS season for which concentrations are below 1850 ppb. These concentrations are highest during the GSS season, coinciding with the bushfire regime in the region. However, it should be noted that fire in tropical forests tend to produce more carbon monoxide (CO) and CH_4 per unit of fuel burned [39]. Frequency and severity of droughts accentuate the occurrence of fire events, and emit large amounts of CH_4 into the atmosphere due to incomplete burning of forest biomass [40,41]. During the year, high concentration values are associated with wind speeds of less than 6 $m.s^{-1}$. In addition, the CPF function (Figure 3c) indicates that only 25% of the concentration values above 1906.1 ppb come mainly from sources of north-west sector in GSP and PSP, and from all directions in GSS. These emission sources of CH_4 are local (i.e., wind speed is <6 $m.s^{-1}$) and are related to the anthropogenic activities above-mentioned. In the GSS season, these

Preprints (www.preprints.org) | NOT PEER-REVIEWED | Posted: 5 September 2023 doi:10.20944/preprints202309.0082.v1

emissions are partly related to Harmattan wind fluxes. These winds blow from north to south carrying desert dust [36,37,42] and polluted air masses due to Sahelian biomass fires [42,43]. Tiemoko et al. [12] showed that these harmattan winds in the GSS season significantly contributed to increased CH_4 concentration and explained ~64% of its variance. In addition, the heat maps of CH_4 concentrations (Figure 3b) show that the significant concentration values during all seasons (> 1970 ppb in GSS, > 1925 ppb in GSP, > 1850 ppb in PSS and > 1950 ppb in PSP) are recorded in the North-West direction with temperature values between 20°C and 26°C. However, at the diurnal scale, a lack of clear and significant correlation between temperature and CH_4 concentrations is found. These observations highlight the complexity of the relationships between these two variables. Indeed, Figure 3 shows variable effects of temperature from one season to another. The distributions of the significant values of CH_4 concentrations are in no way related to any particular variations in temperature.

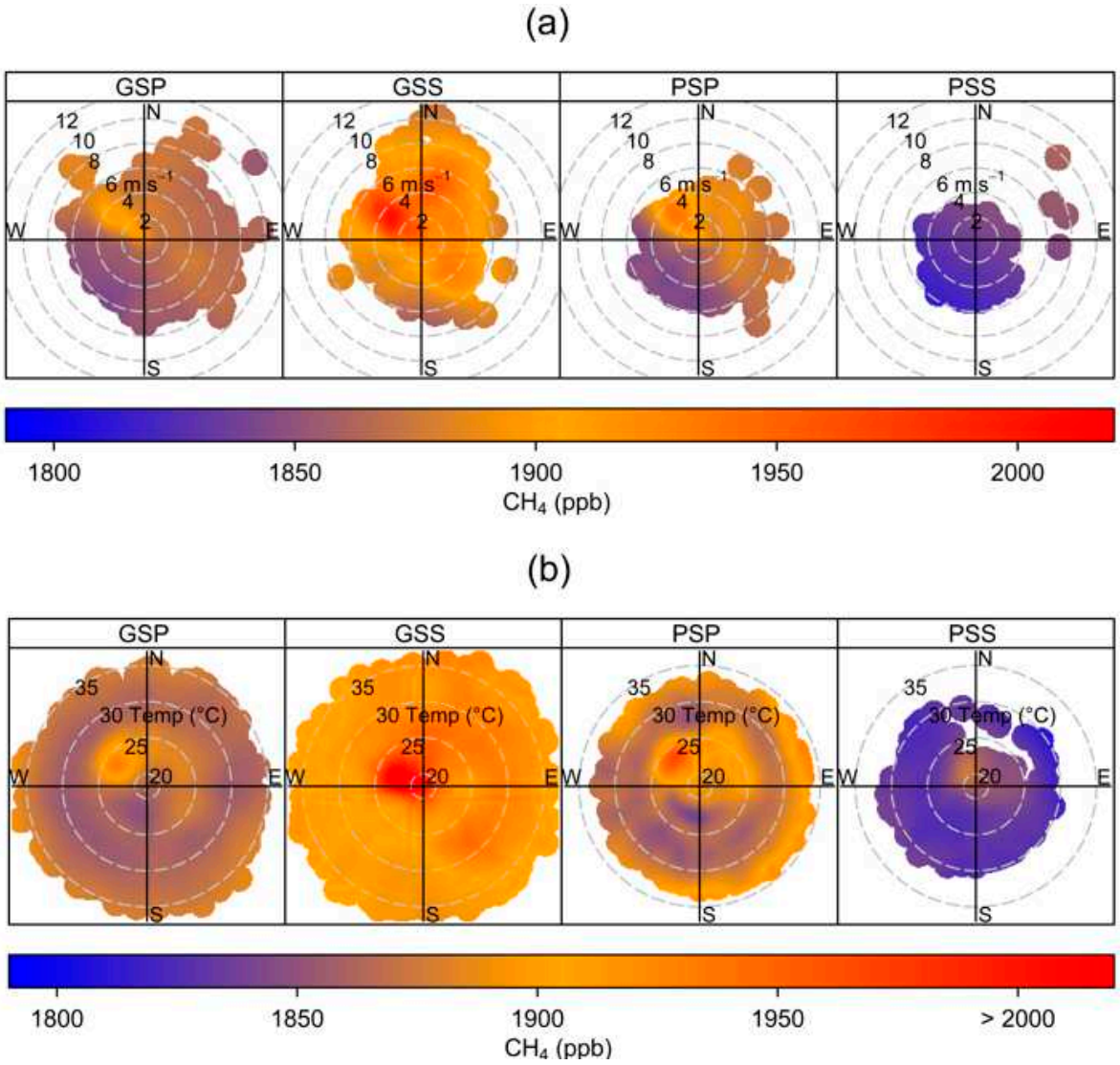

Preprints (www.preprints.org) | NOT PEER-REVIEWED | Posted: 5 September 2023 doi:10.20944/preprints202309.0082.v1

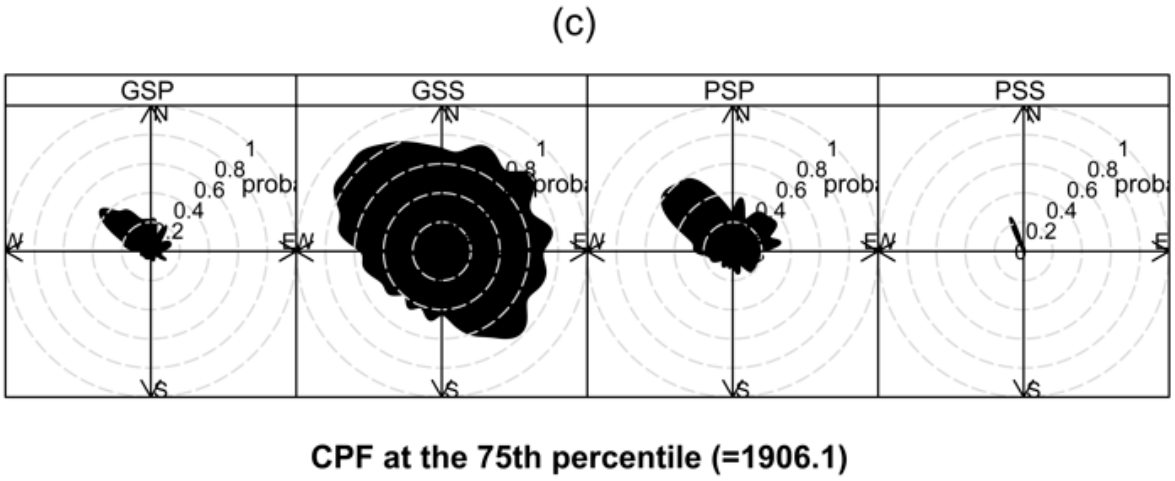

Figure 3. Seasonal bivariate polar plots showing the influence of wind ($m.s^{-1}$, a) and temperature (°C, b), and FPC plots (c) of CH_4 concentrations over the 2014-2018 period at Lamto.

3.2.2. CO_2

Figures 4a and b show two-dimensional polar views of the CO_2 concentrations recorded at Lamto, as a function of wind speed (Figure 4a) and temperature (Figure 4b). Figure 4a shows that the lowest molar fractions of CO_2 are recorded in PSS, which is in accordance with the general annual cycle observed in the work of Tiemoko et al. [4] (see Figure 5a of Tiemoko et al. [4]). On the other hand, the significant CO_2 concentration values (> 420 ppm) are recorded in the GSS, GSP and PSP seasons, and in the north and north-west directions. In these directions, significant concentration values are associated with wind speeds of less than 6 $m.s^{-1}$, which reflect the influences of local emission sources [42]. Similar study [44] has pointed out that the lower the wind speeds (~ 5 $m.s^{-1}$), the higher the concentrations recorded are from local sources. Furthermore, in terms of the contribution of long-range transport, Tiemoko et al. [12] pointed out that continental air flows explain 40% of the variance in CO_2 concentration. These different results show that the local and regional influences on air quality in the Lamto region are predominantly from the north, northeast and northwest sectors, suggesting the main directions of local and regional emission sources. in Figure 4b, it appears clearly that the variations in CO_2 concentrations depend on temperature variations in all directions and in all seasons. In addition, significant CO_2 concentration values (≥ 415 ppm) are associated with areas where the temperature is below 27°C. These observations highlight the effects of the Atmospheric Boundary Layer (ABL) and also the photosynthesis and respiration activities of the vegetation in the CO_2 concentration rate. Indeed, for low temperatures generally at night, dispersed CO_2 plumes are brought down to ground level in stable atmospheric conditions under a contracted boundary layer that induces an accumulation of emissions from local sources. On the other hand, during the day, the high temperatures contribute to dilute the CO_2 concentration rates under an unstable and dilated boundary layer. These observations are also shown in the work of Gu et al. [45] and of Tiemoko et al. [3]. Tiemoko et al. [4] reached the same conclusion in the Lamto area over the 2008-2018 period. They observed a strong contrast between daily and nighttime values of CO_2. Indeed, these authors showed that the temperature is one of the main factors influencing the carbon dioxide produced by vegetation. This influence is significant on the seasonal concentration and its diurnal variation. The Conditional Probability Function (Figure 4c) shows that the over threshold of the 75th percentile is 423.1 ppm. These over thresholds come mainly from sources in the North-West (GSS, GSP and PSP), North-East (GSP, PSP and PSS) and South-East (PSS) sectors, corroborating the previous results.

Preprints (www.preprints.org) | NOT PEER-REVIEWED | Posted: 5 September 2023 doi:10.20944/preprints202309.0082.v1

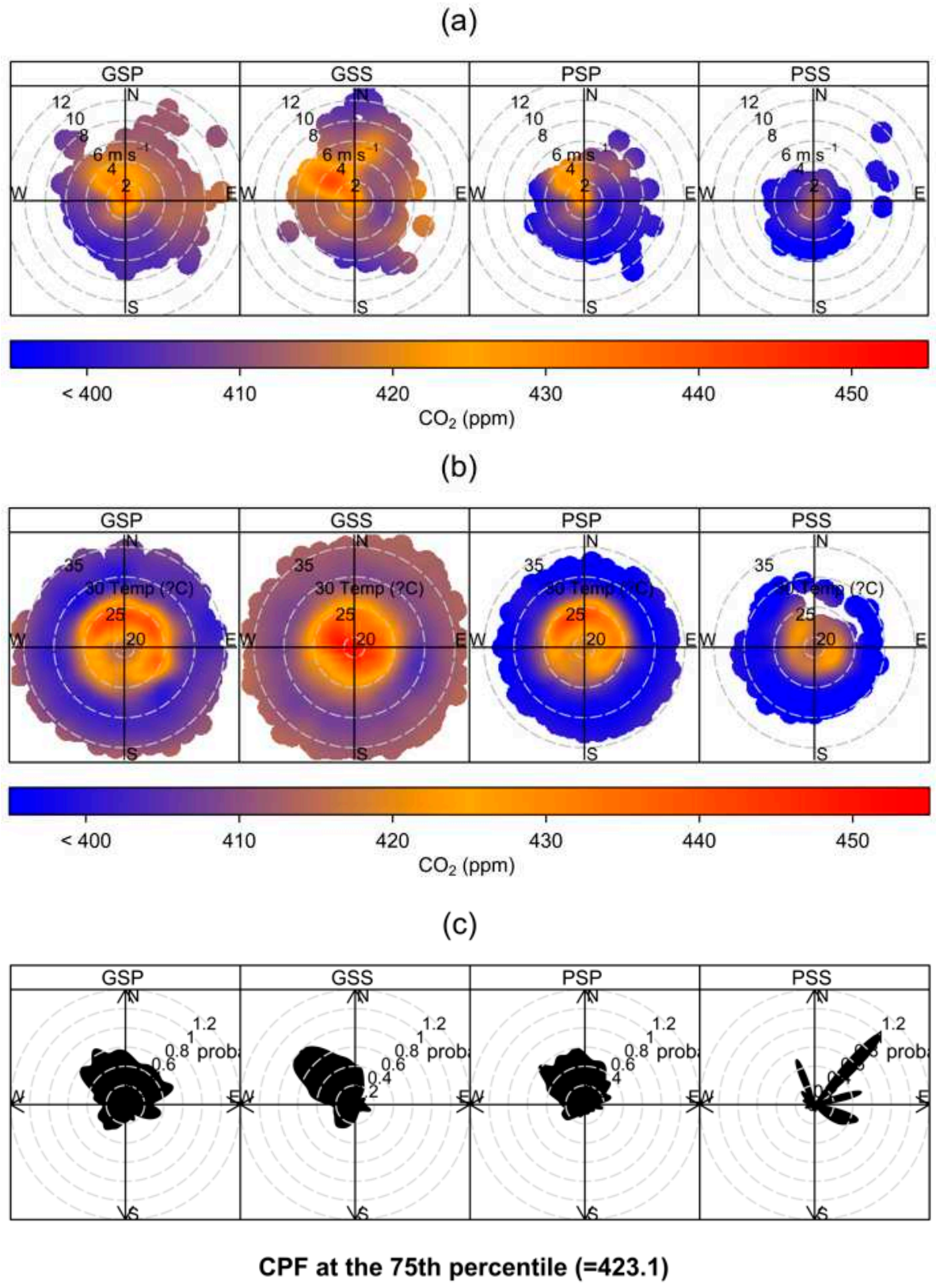

Figure 4. Seasonal bivariate polar plots showing the influence of wind ($m.s^{-1}$, a) and temperature (°C, b), and FPC plots (c) of CO_2 concentrations over the 2014-2018 period at Lamto. .

3.2.3. CO

Figures 5a and b show two-dimensional polar distributions of CO concentrations recorded at Lamto, as a function of temperature (Figure 5b) and wind direction (Figure 5a). Thermal maps for

Preprints (www.preprints.org) | NOT PEER-REVIEWED | Posted: 5 September 2023 doi:10.20944/preprints202309.0082.v1

CO (Figure 5b) show high concentration values (> 225 ppb) in GSS and GSP seasons. In GSP, these significant values are associated with temperatures above 32°C while low concentration values (<225 ppb) are related to temperatures below 32°C. This indicates that the temperature is positively correlated with CO in this season. These observations are also observed over the period from March 12th to April 1st, 2009 in central Christchurch in the middle of the east coast of the Southern Island of New Zealand [46]. This positive correlation between temperature and CO could be attributed to very localized influences (i.e., agricultural burns) that have an impact on local meteorology. Furthermore, in GSS, significant CO concentrations are observed for all temperature ranges, which would indicate the domestic heating influence and also combustion by biomass fires during the season. Indeed, GSS represents the great dry season at Lamto and in this period fire regimes are particularly intense [4,26]. In addition, the highest concentrations (> 375 ppb) come from in the North, North-east, East and East-South sectors. In PSP and PSS seasons, CO concentrations are below 200 ppb for all temperature ranges. These observations could result from the inactivity of potential CO high emission sources. The velocity and wind directions maps (Figure 5a) associated with CO concentrations indicate that the significant concentration values in GSS (> 350 ppb) come from the North, North-west, North-east and East sectors although the winds advection is greater (i.e., prevailing winds) in the South and South-west directions (Figure 1). However, these high concentrations are observed for wind speeds between 1 m.s^{-1} and 9 m.s^{-1}. These observations suggest the existence of two types of sources; local sources characterized by winds velocities below 6 m.s-1 and regional sources for winds velocities above 6 m.s-1. Regional sources are probably associated with a harmattan flow plume carrying polluted air masses over long distances as explained in subsection 3.2.1 in the case of CH_4 [4]. These concentration hot spots in the GSS season are consistent with those observed in the N-W direction for CH_4 and CO_2. This suggests that active emission sources in GSS are similar. In addition, CO concentrations vary very slightly depending on the characteristics of the wind (i.e., wind speed and direction) in the PSS and PSP seasons. The significant CO concentrations in GSP season are between 225 and 300 ppb in the South, North and North-west directions and have a similar distribution to that of GSS. In addition, the seasonal probability function (Figure 5c) at the 85th percentile threshold shows that in GSS and in PSS, the high CO concentrations (≥ 265.6 ppb) have very significant contributions in the North-West, North-East and East-South directions. These different seasonal orientations could be due to the seasonal changes in wind fields [47]. On the other hand, GSP and PSP seasons do not contribute to the 85th percentile threshold of CO concentration levels, which is explained by the fact that anthropogenic activities (e.g., agricultural burns, brush fires), considered as the main source of emissions of CO, are dormant during this period of the year.

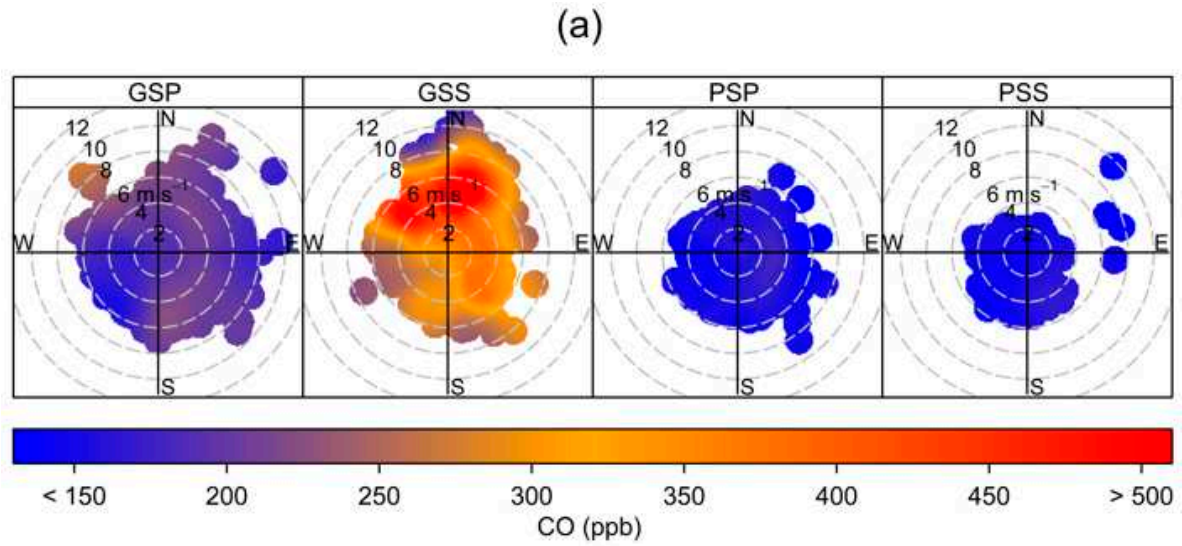

Preprints (www.preprints.org) | NOT PEER-REVIEWED | Posted: 5 September 2023 doi:10.20944/preprints202309.0082.v1

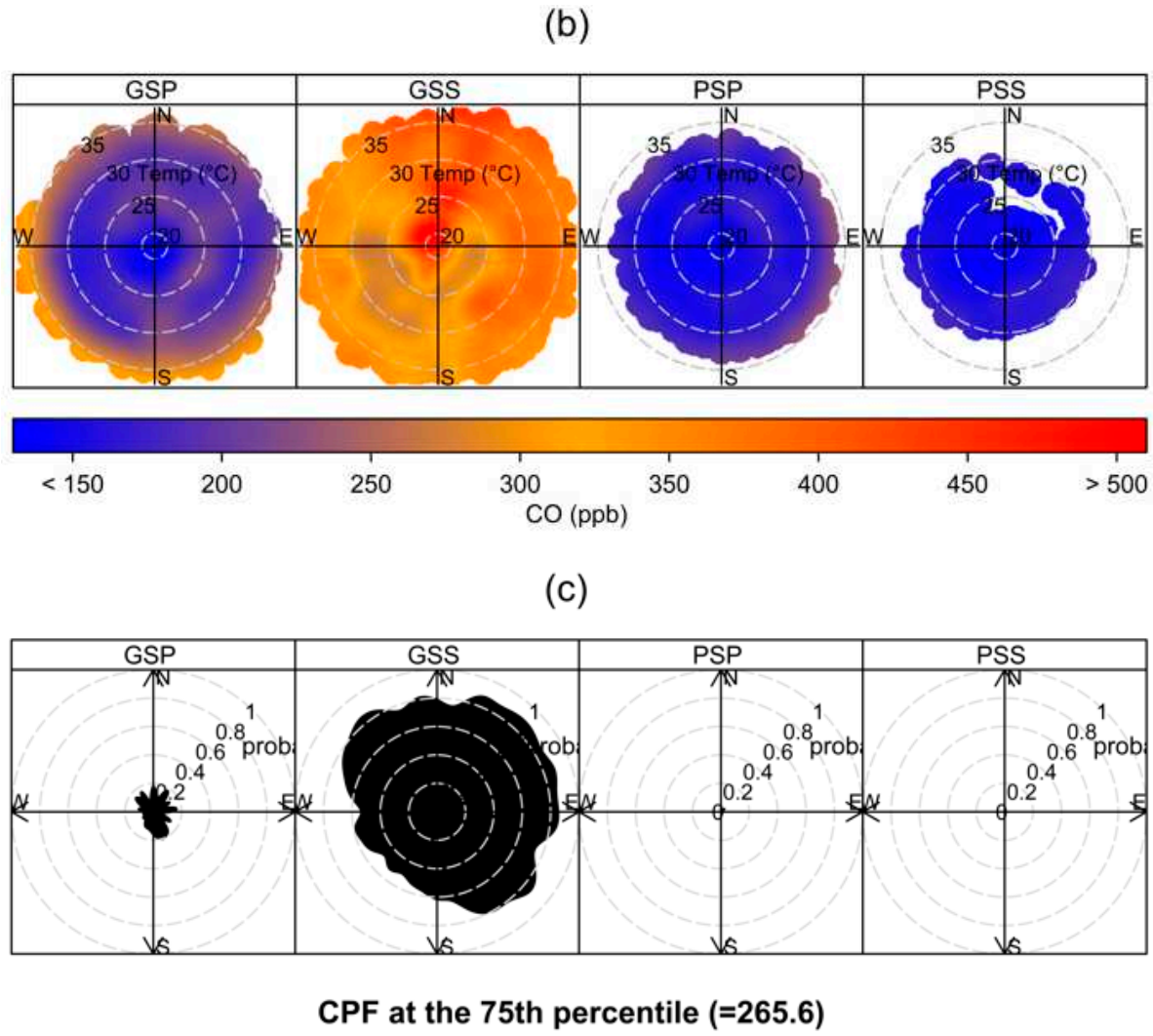

Figure 5. Seasonal bivariate polar plots showing the influence of wind ($m.s^{-1}$, a) and temperature (°C, b), and FPC plots (c) of CO concentrations over the 2014-2018 period at Lamto. .

3.3. Correlation statistic

The correlation statistic is very useful to characterize in this work the behavior of CH_4, CO_2 and CO gases concentration emitted in the atmosphere. Similar emission sources or gases that undergo similar chemical and/or physical transformations in the atmosphere present high and significant correlation values [1]. In addition, Fu et al. [48] emphasized the importance of correlation statistics in assessing the intensity of regional emissions of air pollutants and GHGs. This method also allows the assessment of concentration exchange levels in source-receptor relationships in the observation areas [12,48,49].

The model applied here is the weighted Pearson correlation (R) [50] spatialized by polar diagrams. Polar diagrams allow a simple and more robust analysis of correlations with respect to scatter plots. Indeed, these polar diagrams take into account the local meteorology by providing several correlation values that depend on the climatic variable's behavior used (for example, wind speed and direction).

Figure 6a shows the polar diagram of the correlations between CH_4 and CO obtained as a function of wind speed and direction. The concentrations of CH_4 and CO show high and significant correlations ($R \geq 0.8$; *p-value* < 0.001) in all directions in GSS and in the North-east, South-east and South-west directions in the GSP and PSP seasons. These high and significant correlations show that CH_4 emissions are due to a sum of contributions from various active sources (e.g., livestock, garbage, etc.) alongside biomass combustion that are present in the same season and areas. They are

established for wind speeds lower than 10 m.s-1 in GSS and 12 m.s-1 in GSP seasons. This indicates that similar CH_4 and CO emission sources are both local and distant [4,12]. In PSP season, these high and significant correlations are mainly observed for wind speeds higher than 4 m.s-1. On the other hand, the very low correlations (R< 0.4) are observed during GSS in the Northern direction for wind speeds of ~10 m.s-1, in the North-West and North-East directions in GSP season, for wind speeds of ~2 m.s-1, ~4 m.s-1 and ~9 m.s-1, in the West, North and South-east directions during PSP season, for wind speeds of ~4 m.s-1 and ~5 m.s-1. In PSS, very low correlations are mainly observed for wind speeds below 6 m.s-1 in the West, North-East, East and North-West directions. However, CH_4 emission sources in the North-west sector come from wetlands due to the Taabo hydroelectric dam and Bandama river, whereas those in the North, North-East, South-East and East sectors could come mainly from combustion products. The positive and significant correlations observed between CO and CH_4 at Lamto region, a rural humid savannah area, are believed to be attributable to anthropogenic emissions.

Figure 6b shows the correlations between CO_2 and CO concentrations estimated as a function of wind speed and direction. The observations in these Figure 6b show overall low, but significant (R< 0.5; *p-value* < 0.001) correlation values between CO_2 and CO in all sectors during the GSS and PSP seasons. In GSP season, correlation values are between 0.5 and 0.6. These correlation values in this season are observed in all directions. However, the correlation values obtained for the PSS season are all non-significant, meaning the absence of values in the diagram. We recall that this method only presents the correlation values when the significance is greater than 95 percent (i.e., *p-value < 0.05*). CO_2 and CO emissions in the North-west directions in GSS, and in the North-east directions in GSP and PSP seasons come from both near and far sources while those in PSS are mostly local. Moreover, these correlation variations could be due to the effects of the emission/absorption binomial, which controls the CO_2 concentration rates unlike those of CO. These observations are also shown in the work of Tiemoko et al. [4,12] with correlation values oscillating between 0.21 and 0.63 indicating the influence of terrestrial biosphere fluxes on the atmospheric CO_2 level. Indeed, CO_2 concentrations in the atmosphere may vary due to the biosphere absorption while CO molecules can be removed by the reaction with OH•[51]. The variations of CO_2 and CO concentrations in the atmosphere are therefore due to different processes. Most recently, Tiemoko et al. [4] highlighted a strong monthly variability of the CO_2/CO ratio in Lamto from 2008 to 2018 with maximum and minimum values of around 0.15 ppm/ppb in June and 0.01 ppm/ppb in January respectively. The amplitude between these values is 0.14 ppm/ppb or 93.33% deviation. This high amplitude associated with the additional effects of temperature and wind speed and direction can explain the different correlation variations between CO_2 and CO.

Figure 6c shows the polar diagram of the correlations between CO_2 and CH_4 obtained as a function of wind speed and direction. The correlations are positive, high and significant (R > 0.8; *p-value < 0.001*)) in the North-West, South-West and South-East sectors in GSS, in the North-East sector in GSP and finally in the East-North-West sectors in PSS and PSP seasons. These significant correlations in the different directions can not be clearly explained. However, some studies [52,53] have pointed out that global CO_2 and CH_4 measurements in some sites show significant mixing rates of both gases at high latitudes during winter in the northern hemisphere and then decrease towards the equator. Indeed, because of the persistent latitude gradients, mixing air mass from these different latitudes generates positive correlations between CH_4 and CO_2 [52]. Moreover, the seasonal amplitude values (~13.60 ppm for CO_2 and ~75 ppb for CH_4) calculated in the work of Tiemoko et al. [4] over the 2008-2018 period would indicate also that these emissions are the result of local sources rather than advection of air mass from higher or lower latitudes. These sources although local could be of anthropogenic origin. The significant correlation values calculated in all seasons are associated with both low (< 6 m.s-1) and high (> 6 m.s-1) wind speeds. However, the low correlations obtained for wind speeds less than 6 m.s-1 would result to the effect of the CO_2 absorption by the biosphere on the one hand and/or of the CH_4 emissions from wetlands on the other hand. Thus, the causes of low correlations calculated for wind velocities greater than 6 m.s-1 remain unknown. It should be noted that the air masses analyzed can sometimes cross several areas (cf. work by Tiemoko et al. [12]) and

Preprints (www.preprints.org) | NOT PEER-REVIEWED | Posted: 5 September 2023 doi:10.20944/preprints202309.0082.v1

therefore some of the causes of the correlation's variations could be related to these regions. For example, Touré et al. [37] showed that air masses from Sahelian regions containing dust can reach the Gulf of Guinea. Also, the atmospheric circulation in the lower layers in West Africa shows a predominance of Harmattan flow [12,28,54] from the North and North-east to the coastal regions of the Gulf of Guinea (e.g. Lamto region) during the GSS season. These air masses cross regions considered as relatively important sources of CO_2 and CH_4 high emissions (see Figure 8 of [55]).

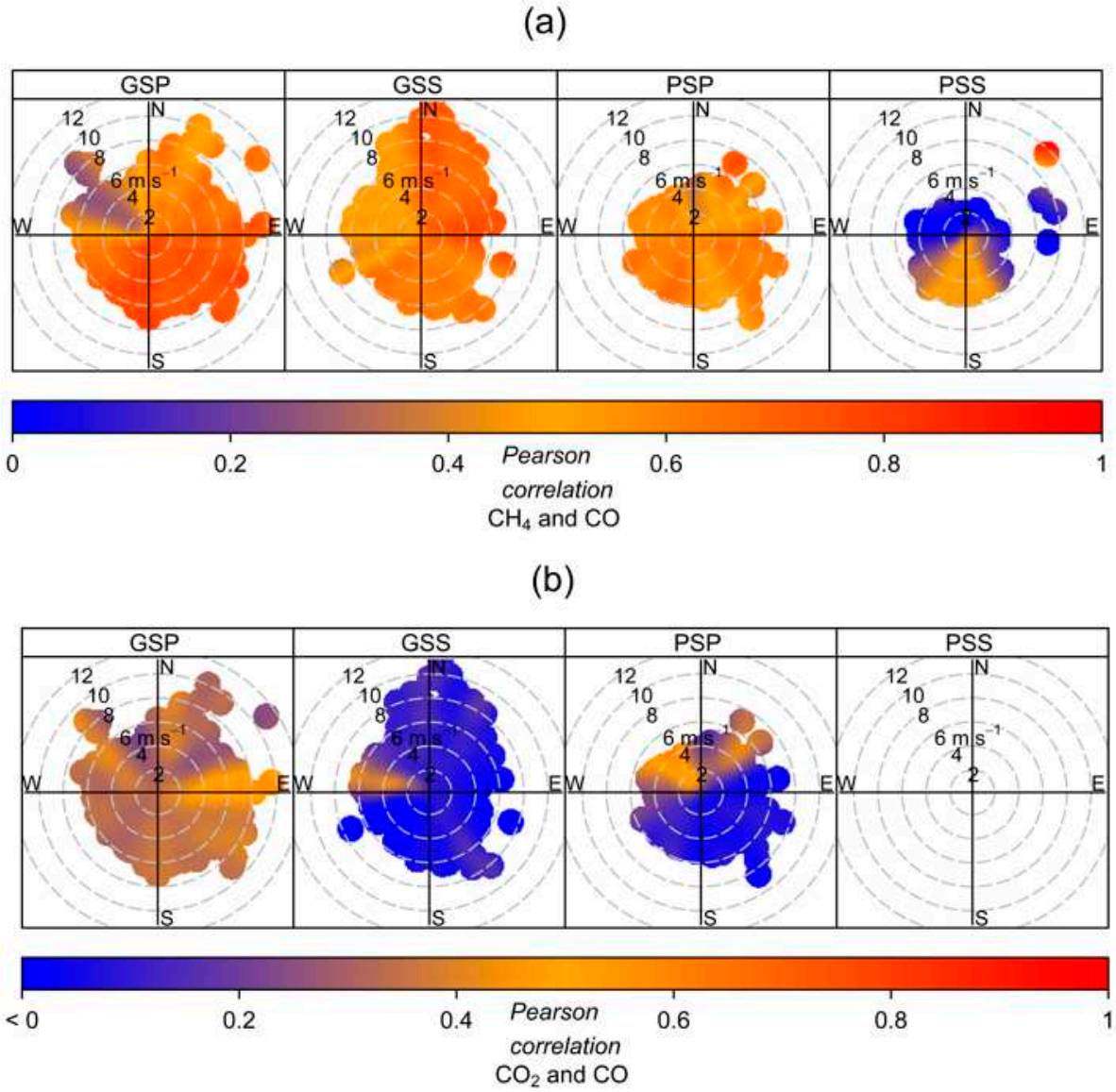

Preprints (www.preprints.org) | NOT PEER-REVIEWED | Posted: 5 September 2023 doi:10.20944/preprints202309.0082.v1

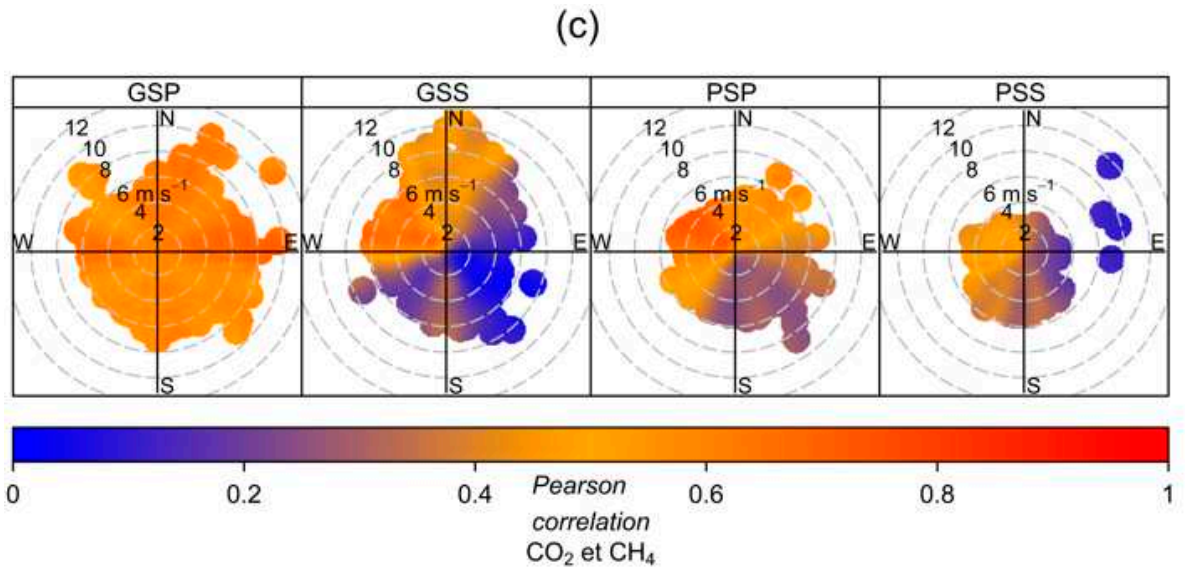

Figure 6. polar diagram of the correlations between CO and CH_4 (a), CO and CO_2 (b), and between CH_4 and CO_2 (c) over the 2014-2018 period at Lamto. .

5. Conclusions

Time series of atmospheric CO_2, CH_4 and CO concentrations recorded at Lamto over the 2014-2018 period were analyzed by seasonal and statistical approach using bivariate polar diagrams and associated CPFs were used with local meteorological parameters (i.e., temperature and wind speed and direction). The significant CO, CO_2 and CH_4 concentration values appear systematically in GSS season. The preferred sectors of significant concentrations are West-North-East directions for CH_4 with wind speeds less than 6 $m.s^{-1}$ during the year. These emission sources are local and related to human activities. Also, the CPF function indicates that 25% of these concentration values come mainly from North-West sector sources associated with temperature between 20°C and 26°C. However, there is no clear and significant correlation between temperature and CH_4 concentration rates.

On the other hand, CO_2 concentrations variations show a certain dependence on temperature variations in all directions and seasons. This highlights the combined effects of the boundary layer and biospheric activities on changes in CO_2 concentrations. Significant concentration values are associated with wind speeds below 6 $m.s^{-1}$ reflecting the influence of local sources.

The CPF shows that concentration over thresholds at the 85th percentile vary significantly from one season to another and come mainly from sources in the North-West (for GSS, GSP and PSP seasons), in the North-East (for GSP, PSP and PSS seasons) and South-East (for PSS season) directions. In addition, thermal maps for CO show that high concentrations during GSP season are associated with temperatures above 32°C and low concentration values are related to temperatures below 32°C. The significant concentrations in GSS are mainly coming from the North, North-east, East and South-east directions with wind speeds between 1 $m.s^{-1}$ and 9 $m.s^{-1}$. The emission sources are both local and regional, and the large-scale impact is the incursion of the harmattan flow that carries polluted air masses from long distances. Correlation coefficients calculated between pairs of gases show very significant correlations (≥ 0.8) between CH_4 and CO in all directions in GSS season, and in the North-east, South-east and South-west directions in GSP and PSP seasons for wind speeds less than 10 $m.s^{-1}$ (for GSS) and less than 12 $m.s^{-1}$ (for GSP). These correlations indicate a similarity between the CO and CH_4 emission sources in all sectors. These emission sources are both local and regional. On the other hand, CO and CO_2 concentrations show very significant correlations in the North-West directions in GSS, and in the North-East in GSP and PSP seasons. However, in PSS, the correlations are low and the emission sources are mainly local. Furthermore, the positive and significant correlations (> 0.8) calculated between CO_2 and CH_4 are present in the North-West, South-West and

South-East sectors in GSS, in the North-East sector in GSP and finally in the East-North-West sectors in PSS and PSP seasons. These correlation values are associated with both low (< 6 $m.s^{-1}$) and high (> 6 $m.s^{-1}$) wind speeds, while low correlations are obtained for wind speeds above 6 $m.s^{-1}$. In addition, bivariate polar plots methods that take into account the local meteorological variables, particularly wind speed and direction, are certainly effective in determining the directions of gases emission, but wind analysis can not be directly associated with a distance in order to right locate the sources. Thus, the implementation of other methods to determine the distance between the receiver (i.e., measurement point) and the transmitter (i.e., source) would improve interpretations and better affect the location of local sources.

Author Contributions: Conceptualization, D.T.T., F.Y., and M.R.; methodology, D.T.T., F.Y., and K.K.B; software, D.T.T.; validation, F.Y., and K.K.B; formal analysis, D.T.T.; investigation, D.T.T.; data curation, M.R.; writing—original draft preparation, D.T.T.; writing—review and editing, F.Y., F.D.B.B, A.L.M.Y., A.D., K.K.B, k.k.; and A.K.; supervision, A.D. and M.R. All authors have read and agreed to the published version of the manuscript.

Acknowledgments: The authors are grateful to the Geophysical Station of Lamto and the "Laboratoire des Sciences du Climat et de l'Environnement" (LSCE-Paris) for their technical support.

Conflicts of Interest: The authors declare no conflict of interest.

References

1. Grange, S.K.; Lewis, A.C.; Carslaw, D.C. Source Apportionment Advances Using Polar Plots of Bivariate Correlation and Regression Statistics. *Atmos. Environ.* **2016**, *145*, 128–134, doi: 10.1016/j.atmosenv.2016.09.016.
2. Mai, B.; Deng, X.; Liu, X.; Li, T.; Guo, J.; Ma, Q. The Climatology of Ambient CO2 Concentrations from Long-Term Observation in the Pearl River Delta Region of China: Roles of Anthropogenic and Biogenic Processes. *Atmos. Environ.* **2021**, *251*, 118266, doi: 10.1016/j.atmosenv.2021.118266.
3. Tiemoko, D.T.; Yoroba, F.; Diawara, A.; Kouadio, K.; Kouassi, B.K.; Yapo, A.L.M. Understanding the Local Carbon Fluxes Variations and Their Relationship to Climate Conditions in a Sub-Humid Savannah-Ecosystem during 2008-2015: Case of Lamto in Cote d'Ivoire. *Atmospheric Clim. Sci.* **2020**, *10*, 186–205, doi:10.4236/acs.2020.102010.
4. Tiemoko, T.D.; Ramonet, M.; Yoroba, F.; Kouassi, K.B.; Kouadio, K.; Kazan, V.; Kaiser, C.; Truong, F.; Vuillemin, C.; Delmotte, M.; et al. Analysis of the Temporal Variability of CO_2, CH_4 and CO Concentrations at Lamto, West Africa. *Tellus B Chem. Phys. Meteorol.* **2021**, *73*, 1863707, doi:10.1080/16000889.2020.1863707.
5. Statheropoulos, M.; Vassiliadis, N.; Pappa, A. Principal Component and Canonical Correlation Analysis for Examining Air Pollution and Meteorological Data. *Atmos. Environ.* **1998**, *32*, 1087–1095, doi:10.1016/S1352-2310(97)00377-4.
6. Manoli, E.; Voutsa, D.; Samara, C. Chemical Characterization and Source Identification/Apportionment of Fine and Coarse Air Particles in Thessaloniki, Greece. *Atmos. Environ.* **2002**, *36*, 949–961, doi:10.1016/S1352-2310(01)00486-1.
7. Donnelly, A.; Misstear, B.; Broderick, B. Application of Nonparametric Regression Methods to Study the Relationship between NO_2 Concentrations and Local Wind Direction and Speed at Background Sites. *Sci. Total Environ.* **2011**, *409*, 1134–1144, doi: 10.1016/j.scitotenv.2010.12.001.
8. Malby, A.R.; Whyatt, J.D.; Timmis, R.J. Conditional Extraction of Air-Pollutant Source Signals from Air-Quality Monitoring. *Atmos. Environ.* **2013**, *74*, 112–122, doi: 10.1016/j.atmosenv.2013.03.028.
9. Petit, J.-E.; Favez, O.; Albinet, A.; Canonaco, F. A User-Friendly Tool for Comprehensive Evaluation of the Geographical Origins of Atmospheric Pollution: Wind and Trajectory Analyses. *Environ. Model. Softw.* **2017**, *88*, 183–187, doi: 10.1016/j.envsoft.2016.11.022.
10. Henne, S.; Klausen, J.; Junkermann, W.; Kariuki, J.M.; Aseyo, J.O.; Buchmann, B. Representativeness and Climatology of Carbon Monoxide and Ozone at the Global GAW Station Mt. Kenya in Equatorial Africa. *Atmospheric Chem. Phys.* **2008**, *8*, 3119–3139, doi:10.5194/acp-8-3119-2008.
11. Ncipha, X.G.; Sivakumar, V.; Malahlela, O.E. The Influence of Meteorology and Air Transport on CO2 Atmospheric Distribution over South Africa. *Atmosphere* **2020**, *11*, 287, doi:10.3390/atmos11030287.
12. Tiemoko, D.T.; Yoroba, F.; Paris, J.-D.; Diawara, A.; Berchet, A.; Pison, I.; Riandet, A.; Ramonet, M. Source–Receptor Relationships and Cluster Analysis of CO_2, CH_4, and CO Concentrations in West Africa: The Case of Lamto in Côte d'Ivoire. *Atmosphere* **2020**, *11*, 903, doi:10.3390/atmos11090903.
13. Rosa, L.P.; Schaeffer, R. Greenhouse Gas Emissions from Hydroelectric Reservoirs. *Ambio* **1994**, *23*, 164–165.

14. Galy-Lacaux, C.; Delmas, R.; Kouadio, G.; Richard, S.; Gosse, P. Long-Term Greenhouse Gas Emissions from Hydroelectric Reservoirs in Tropical Forest Regions. *Glob. Biogeochem. Cycles* **1999**, *13*, 503–517.
15. Galy-Lacaux, C.; Delmas, R.; Jamber, C.; Dumestre, J.-F.; Labroue, L.; Richard, S.; Gosse, P. Gaseous Emissions and Oxygen Consumption in Hydroelectric Dams: A Case Study in French Guiana. *Glob. Biogeochem. Cycles.* **1997**, *11*, 471–183.
16. Delmas, R.; Galy-Lacaux, C.; Richard, S. Emissions of Greenhouse Gases from the Tropical Hydroelectric Reservoir of Petit Saut (French Guiana) Compared with Emissions from Thermal Alternatives. *Glob. Biogeochem. Cycles* **2001**, *15*, 993–1003, doi:10.1029/2000GB001330.
17. Carslaw, D.; Beevers, S.; Ropkins, K.; Bell, M. Detecting and Quantifying Aircraft and Other On-Airport Contributions to Ambient Nitrogen Oxides in the Vicinity of a Large International Airport. *Atmos. Environ.* **2006**, *40*, 5424–5434, doi: 10.1016/j.atmosenv.2006.04.062.
18. Uria-Tellaetxe, I.; Carslaw, D.C. Conditional Bivariate Probability Function for Source Identification. *Environ. Model. Softw.* **2014**, *59*, 1–9, doi: 10.1016/j.envsoft.2014.05.002.
19. Carslaw, D.C.; Ropkins, K. Openair — An R Package for Air Quality Data Analysis. *Environ. Model. Softw.* **2012**, *27–28*, 52–61, doi: 10.1016/j.envsoft.2011.09.008.
20. Szulecka, A.; Oleniacz, R.; Rzeszutek, M. Functionality of Openair Package in Air Pollution Assessment and Modeling — a Case Study of Krakow. *Ochr. Srodowiska Zasobów Nat.* **2017**, *28*, 22–27, doi:10.1515/oszn-2017-0009.
21. Boon, A.; Broquet, G.; Clifford, D.J.; Chevallier, F.; Butterfield, D.M.; Pison, I.; Ramonet, M.; Paris, J.D.; Ciais, P. Analysis of the Potential of near Ground Measurements of CO_2 and CH_4 in London, UK for the Monitoring of City-Scale Emissions Using an Atmospheric Transport Model. Atmos. Chem. Phys.**2016**, 16, 6735-6756, doi: 10.5194/acp-16-6735-2016
22. Buchholz, R.R.; Paton-Walsh, C.; Griffith, D.W.T.; Kubistin, D.; Caldow, C.; Fisher, J.A.; Deutscher, N.M.; Kettlewell, G.; Riggenbach, M.; Macatangay, R.; et al. Source and Meteorological Influences on Air Quality (CO, CH_4 & CO_2) at a Southern Hemisphere Urban Site. *Atmos. Environ.* **2016**, *126*, 274–289, doi: 10.1016/j.atmosenv.2015.11.041.
23. Bae, M.-S.; Schwab, J.J.; Chen, W.-N.; Lin, C.-Y.; Rattigan, O.V.; Demerjian, K.L. Identifying Pollutant Source Directions Using Multiple Analysis Methods at a Rural Location in New York. *Atmos. Environ.* **2011**, *45*, 2531–2540, doi: 10.1016/j.atmosenv.2011.02.020.
24. Munir, S.; Habeebullah, T.M.; Mohammed, A.M.F.; Morsy, E.A.; Rehan, M.; Ali, K. Analysing PM2.5 and Its Association with PM10 and Meteorology in the Arid Climate of Makkah, Saudi Arabia. *Aerosol Air Qual. Res.* **2017**, *17*, 453–464, doi:10.4209/aaqr.2016.03.0117.
25. GIEC Changement Climatique 2014: rapport De Synthèse. Contribution Des Groupes De Travail I, II Et III au Cinquième Rapport D'évaluation du Groupe D'experts Intergouvernemental Sur L'évolution du Climat [Sous la Direction De L'équipe De Rédaction Principale (R.K. Pachauri, L.A. Meyer, eds.).; Genève, Suisse, 2014; p. 161.
26. Diawara, A.; Yoroba, F.; Kouadio, K.Y.; Kouassi, K.B.; Assamoi, E.M.; Diedhiou, A.; Assamoi, P. Climate Variability in the Sudano-Guinean Transition Area and Its Impact on Vegetation: The Case of the Lamto Region in Côte D'Ivoire. *Adv. Meteorol.* **2014**, *2014*, 1–11, doi:10.1155/2014/831414.
27. Devineau, J.-L. Etude quantitative des forêts-galeries de Lamto (Moyenne Côte d'Ivoire). Thesis, Université Pierre et Marie Curie-Paris VI.: Paris, 1975.
28. Louvet Modulations intrasaisonnières de la mousson d'Afrique de l'Ouest et impacts sur les vecteurs du paludisme à Ndiop (Sénégal): diagnostics et prévisibilité. PhD Thesis, Université de Bourgogne: France, 2008.
29. Nacro, H.B. Le Feu de Brousse, Un Facteur de Reproduction Des Écosystèmes de Savanes à Dominance Herbacées à Lamto (Côte d'Ivoire). *Rev CAMES-Sér A.* **2003**, *2*, 49–54.
30. Carslaw, D.C.; Ropkins, K. Openair — An R Package for Air Quality Data Analysis. *Environ. Model. Softw.* **2012**, *27–28*, 52–61, doi: 10.1016/j.envsoft.2011.09.008.
31. Carslaw, D.C.; Beevers, S.D. Characterising and Understanding Emission Sources Using Bivariate Polar Plots and K-Means Clustering. *Environ. Model. Softw.* **2013**, *40*, 325–329, doi: 10.1016/j.envsoft.2012.09.005.
32. Ashbaugh, L.L.; Malm, W.C.; Sadeh, W.Z. A Residence Time Probability Analysis of Sulfur Concentrations at Grand Canyon National Park. *Atmospheric Environ. 1967* **1985**, *19*, 1263–1270, doi:10.1016/0004-6981(85)90256-2.
33. Tong, L.; Zhang, J.; Xiao, H.; Cai, Q.; Huang, Z.; Zhang, H.; Zheng, J.; He, M.; Peng, C.; Feng, J.; et al. Identification of the Potential Regions Contributing to Ozone at a Coastal Site of Eastern China with Air Mass Typology. *Atmospheric Pollut. Res.* **2017**, *8*, 1044–1057, doi: 10.1016/j.apr.2017.04.005.
34. Zhou, S.; Davy, P.K.; Huang, M.; Duan, J.; Wang, X.; Fan, Q.; Chang, M.; Liu, Y.; Chen, W.; Xie, S.; et al. High-Resolution Sampling and Analysis of Ambient Particulate Matter in the Pearl River Delta Region of Southern China: Source Apportionment and Health Risk Implications. *Atmospheric Chem. Phys.* **2018**, *18*, 2049–2064, doi:10.5194/acp-18-2049-2018.

35. Vellingiri, K.; Kim, K.-H.; Lim, J.-M.; Lee, J.-H.; Ma, C.-J.; Jeon, B.-H.; Sohn, J.-R.; Kumar, P.; Kang, C.-H. Identification of Nitrogen Dioxide and Ozone Source Regions for an Urban Area in Korea Using Back Trajectory Analysis. *Atmospheric Res.* **2016**, *176–177*, 212–221, doi: 10.1016/j.atmosres.2016.02.022.
36. Rodríguez, S.; Alastuey, A.; Alonso-Pérez, S.; Querol, X.; Cuevas, E.; Abreu-Afonso, J.; Viana, M.; Pérez, N.; Pandolfi, M.; De La Rosa, J. Transport of Desert Dust Mixed with North African Industrial Pollutants in the Subtropical Saharan Air Layer. *Atmospheric Chem. Phys.* **2011**, *11*, 6663–6685, doi:10.5194/acp-11-6663-2011.
37. Touré, N.E.; Konaré, A.; Silué, S. Intercontinental Transport and Climatic Impact of Saharan and Sahelian Dust. *Adv. Meteorol.* **2012**, *2012*, 1–14, doi:10.1155/2012/157020.
38. Adler, B.; Babić, K.; Kalthoff, N.; Lohou, F.; Lothon, M.; Dione, C.; Pedruzo-Bagazgoitia, X.; Andersen, H. Nocturnal Low-Level Clouds in the Atmospheric Boundary Layer over Southern West Africa: An Observation-Based Analysis of Conditions and Processes. *Atmospheric Chem. Phys.* **2019**, *19*, 663–681, doi:10.5194/acp-19-663-2019.
39. De Souza Maria, L.; Rossi, F.S.; Costa, L.M.D.; Campos, M.O.; Blas, J.C.G.; Panosso, A.R.; Silva, J.L.D.; Silva Junior, C.A.D.; La Scala Jr, N. Spatiotemporal Analysis of Atmospheric XCH4 as Related to Fires in the Amazon Biome during 2015–2020. *Remote Sens. Appl. Soc. Environ.* **2023**, *30*, 100967, doi: 10.1016/j.rsase.2023.100967.
40. Anderson, L.O.; Ribeiro Neto, G.; Cunha, A.P.; Fonseca, M.G.; Mendes De Moura, Y.; Dalagnol, R.; Wagner, F.H.; De Aragão, L.E.O.E.C. Vulnerability of Amazonian Forests to Repeated Droughts. *Philos. Trans. R. Soc. B Biol. Sci.* **2018**, *373*, 20170411, doi:10.1098/rstb.2017.0411.
41. Basso, L.S.; Marani, L.; Gatti, L.V.; Miller, J.B.; Gloor, M.; Melack, J.; Cassol, H.L.G.; Tejada, G.; Domingues, L.G.; Arai, E.; et al. Amazon Methane Budget Derived from Multi-Year Airborne Observations Highlights Regional Variations in Emissions. *Commun. Earth Environ.* **2021**, *2*, 246, doi:10.1038/s43247-021-00314-4.
42. Nho, E.-Y.; Ardouin, B.; Le Cloarec, M.F.; Ramonet, M. Origins of 210Po in the Atmosphere at Lamto, Ivory Coast: Biomass Burning and Saharan Dusts. *Atmos. Environ.* **1996**, *30*, 3705–3714, doi:10.1016/1352-2310(96)00093-3.
43. Capes, G.; Johnson, B.; McFiggans, G.; Williams, P.I.; Haywood, J.; Coe, H. Aging of Biomass Burning Aerosols over West Africa: Aircraft Measurements of Chemical Composition, Microphysical Properties, and Emission Ratios. *J. Geophys. Res.* **2008**, *113*, D00C15, doi:10.1029/2008JD009845.
44. Morgan, L. Estimation des émissions de gaz à effet de serre à différentes échelles en France à l'aide d'observations de haute précision. PhD Thesis, Université Paris Sud-Paris XI: Paris, 2012.
45. Gu, H.; Yu, Z.W.; Xu, D.W.; Huang, Y.; Zheng, L.; Ma, J. Seasonal Dynamics of Carbon Dioxide Concentration and Its Influencing Factors in Urban Park Green Spaces in Northeast China. *Nat. Environ. Pollut. Technol.* **2018**, *17*, 329–337.
46. Pattinson, W.; Kingham, S.; Longley, I.; Salmond, J. Potential Pollution Exposure Reductions from Small-Distance Bicycle Lane Separations. *J. Transp. Health* **2017**, *4*, 40–52, doi: 10.1016/j.jth.2016.10.002.
47. Sultan, B.; Janicot, S. La Variabilité Climatique En Afrique de l'Ouest Aux Échelles Saisonnière et Intra-Saisonnière. I: Mise En Place de La Mousson et Variabilité Intra-Saisonnière de La Convection. *Sci. Chang. Planétaires Sécheresse* **2004**, *15*, 321–330.
48. Fu, X.W.; Zhang, H.; Lin, C.-J.; Feng, X.B.; Zhou, L.X.; Fang, S.X. Correlation Slopes of GEM / CO, GEM / CO_2, and GEM / CH_4 and Estimated Mercury Emissions in China, South Asia, the Indochinese Peninsula, and Central Asia Derived from Observations in Northwestern and Southwestern China. *Atmospheric Chem. Phys.* **2015**, *15*, 1013–1028, doi:10.5194/acp-15-1013-2015.
49. Tohjima, Y.; Kubo, M.; Minejima, C.; Mukai, H.; Tanimoto, H.; Ganshin, A.; Maksyutov, S.; Katsumata, K.; Machida, T.; Kita, K. Temporal Changes in the Emissions of CH_4 and CO from China Estimated from CH_4/CO_2 and CO/CO_2 correlations Observed at Hateruma Island. *Atmospheric Chem. Phys.* **2014**, *14*, 1663–1677, doi:10.5194/acp-14-1663-2014.
50. Canty, A.; Ripley, B. Boot: Bootstrap R (S-Plus) Functions. R Package Version 1.3-28.1. **2022**.
51. Bechara, J. Impact de la mousson sur la chimie photo oxydante en Afrique de l'Ouest Thèse de Doctorat., Université Paris-Est: Paris, 2009.
52. Conway, T.J.; Steele, L.P.; Novelli, P.C. Correlations among Atmospheric CO_2, CH_4 and CO in the Arctic, March 1989. *Atmospheric Environ. Part Gen. Top.* **1993**, *27*, 2881–2894, doi:10.1016/0960-1686(93)90319-T.
53. Steele, L.P.; Fraser, P.J.; Rasmussen, R.A.; Khalil, M.A.K.; Conway, T.J.; Crawford, A.J.; Gammon, R.H.; Masarie, K.A.; Thoning, K.W. The Global Distribution of Methane in the Troposphere. *J. Atmospheric Chem.* **1987**, *5*, 125–171, doi:10.1007/BF00048857.
54. Yoroba, F.; Diawara, A.; Kouadio, K.Y.; Schayes, G.; Assamoi, A.P.; Kouassi, K.B.; Kouassi, A.A.; Toualy, E. Analysis of the West African Rainfall Using a Regional Climate Model. *Int. J. Environ. Sci.* **2011**, *1*, 1339–1349.
55. Van Der Werf, G.R.; Randerson, J.T.; Giglio, L.; Van Leeuwen, T.T.; Chen, Y.; Rogers, B.M.; Mu, M.; Van Marle, M.J.E.; Morton, D.C.; Collatz, G.J.; et al. Global Fire Emissions Estimates during 1997–2016. *Earth Syst. Sci. Data*. **2017**, *9*, 697–720, doi:10.5194/essd-9-697-2017.